

EFFICIENT LUNG ULTRASOUND SEVERITY SCORING USING DEDICATED FEATURE EXTRACTOR

Jiaqi Guo^{1†}, Yunan Wu¹, Evangelos Kaimakamis², Georgios Petmezas³, Vasileios E. Papageorgiou³,
Nicos Maglaveras³, Aggelos K. Katsaggelos^{1†}

¹ Northwestern University, Illinois, USA

² "G. Papanikolaou" General Hospital, Thessaloniki, GREECE

³ Aristotle University, Thessaloniki, GREECE

ABSTRACT

With the advent of the COVID-19 pandemic, ultrasound imaging has emerged as a promising technique for COVID-19 detection, due to its non-invasive nature, affordability, and portability. In response, researchers have focused on developing AI-based scoring systems to provide real-time diagnostic support. However, the limited size and lack of proper annotation in publicly available ultrasound datasets pose significant challenges for training a robust AI model. This paper proposes MeDiVLAD, a novel pipeline to address the above issue for multi-level lung-ultrasound (LUS) severity scoring. In particular, we leverage self-knowledge distillation to pre-train a vision transformer (ViT) *without label* and aggregate frame-level features via *dual-level VLAD aggregation*. We show that with minimal finetuning, MeDiVLAD outperforms conventional fully-supervised methods in both frame- and video-level scoring, while offering classification reasoning with exceptional quality. This superior performance enables key applications such as the automatic identification of critical lung pathology areas and provides a robust solution for broader medical video classification tasks.¹

Index Terms— Deep Neural Network, DINO, VLAD, Medical Video Classification, Lung Ultrasound Score

1. INTRODUCTION

The LUS score is a crucial tool for assessing lung disease severity [1], particularly helpful for non-expert practitioners in evaluating patients with pulmonary abnormalities in unsupervised settings. AI-based LUS scoring typically involves extracting frame-level features with a pretrained deep neural network (DNN), then aggregating them into video-level

embeddings. This method faces two challenges: **Network Pretraining**: Limited public LUS datasets, varying acquisition systems, image quality, and lack of annotations hinder the effectiveness of traditional supervised learning. **Frame-level Aggregation**: Aggregating frame-level features risks information loss, making it crucial to retain key details for optimal LUS performance. To address the first challenge, several AI-based scoring methods leverage contrastive learning [2, 3, 4], which learns discriminative features by promoting intra-class similarity. However, most of these approaches rely on costly expert annotations for training. Interestingly, we identify a similar solution in self-supervised learning (SSL) methods, which can be trained without labels and have demonstrated potential in image processing [5, 6, 7, 8]. Among these methods, DINO [8] stands out by leveraging a Vision Transformer (ViT) to learn representations through self-knowledge distillation, enabling the training of self-attention mechanisms with limited data. This makes DINO an ideal candidate for pretraining feature extractors in frame-level tasks.

For the second challenge, a straightforward method is to apply the maximum frame-level probability across the video [4], classifying based on the most prominent frame in the video. Other frame-level feature aggregations in video classification are commonly addressed using two paradigms. The first employs recurrent neural networks (RNNs) [9] to model the temporal dynamics of video sequences, deriving an overall representation from the frame-level features. The second paradigm, broadly categorized as the Bag-of-Visual-Words (BoVW) based aggregation, constructs local frame descriptors, assigns them to pre-defined clusters, and aggregates their residuals into a global representation. A common example of this approach is VLAD [10] and its variants [11, 12]. Other methods, such as I3D [13], which relies on 3D convolutions, are computationally expensive. In comparison, we believe BoVW-based aggregation will be more suitable for our task than RNN-based methods, as LUS video labels often depend on several typical frames within a short time frame, making temporal dependencies less significant.

In this paper, we proposed a semi-self-supervised learn-

© 20XX IEEE. Personal use of this material is permitted. Permission from IEEE must be obtained for all other uses, in any current or future media, including reprinting/republishing this material for advertising or promotional purposes, creating new collective works, for resale or redistribution to servers or lists, or reuse of any copyrighted component of this work in other works.

[†] Corresponding author.

¹Code: <https://github.com/GuoJiaqi-1020/MeDiVLAD>

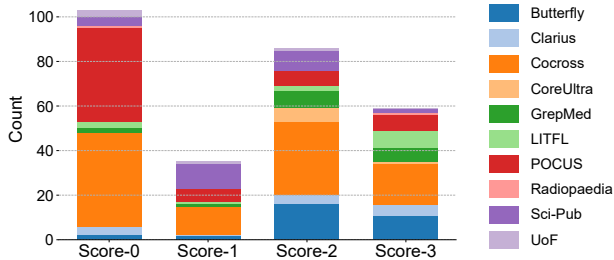


Fig. 1. Score distribution of our LUS dataset, with different colors indicating different data sources. CoCross is our private dataset, other sources are detailed in [15]

ing pipeline, **MeDiVLAD**, for accurate LUS severity scoring. Our method utilizes self-knowledge distillation to pretrain a ViT backbone without labels and finetune it with minimal supervision. To capture both temporal and spatial patterns, we introduce a VLAD-based dual-level assignment matrix for aggregating frame-level features. Remarkably, even without supervised finetuning, the pretrained ViT surpasses a fully supervised ResNet50 on the frame-level LUS task, with its attention map demonstrating precise classification reasoning. At the video-level, MeDiVLAD outperforms both LSTM [14] and NetVLAD [11] aggregation, achieving superior performance in the video-level scoring.

2. DATA & PROBLEM STATEMENT

We curated our LUS dataset with 177 curvilinear ultrasound videos from the COVIDx-US [15] dataset and 106 ultrasound videos collected from "G. Papanikolaou" General Hospital of Thessaloniki (CoCross), totaling 283 videos from 156 patients. The data distribution is shown in Fig 1. To improve frame-level scoring, we randomly selected 2 – 3 representative frames from each video, resulting in a small frame-level dataset of 585 annotated images.

We adopt an **improved LUS scoring system**, namely the integrated lung ultrasound score (i-LUS)[16]. This system incorporates additional factors such as pleural line characteristics and cardiac involvement in COVID-19, providing a more comprehensive assessment. I-LUS uses a 4-level scoring system: **Score-0** represents a normal lung with a continuous pleural line and horizontal A-line artifact; **Score-1** indicates at least 2 isolated or coalescent B-lines covering less than 50% of the image without clear sub-pleural alterations; **Score-2** includes B-lines covering more than 50% of the image, still without clear sub-pleural alterations; and **Score-3** represents consolidation with poorly dynamic arborescent air bronchograms. Considering the extreme class imbalance in our dataset, **we combined scores 1 and 2, simplifying it to a 3-level scoring system**. Given such a three score system $\mathbf{Y} \in \{y_0, y_1, y_2\}$ and a ultrasound video containing N frames, $\mathbf{V} \in \{\mathbf{x}_0, \mathbf{x}_1, \dots, \mathbf{x}_{N-1}\}$, our goal is to predict

the probability $p(y_i|\mathbf{x})$ for a single frame \mathbf{x} , and $p(y_i|\mathbf{V})$ for the entire video \mathbf{V} . These probabilities are parameterized using two different neural networks ϕ_i and ϕ_v , where $\phi_i(\mathbf{x}) = p(y_i|\mathbf{x})$ and $\phi_v(\mathbf{x}_0, \mathbf{x}_1, \dots, \mathbf{x}_{N-1}) = p(y_i|\mathbf{V})$. For simplicity, all videos are reshaped to 224×224 and uniformly downsampled to $N = 15$ frames. For samples with fewer than 15 frames, nearest-neighbor interpolation is applied to match the target frame count.

3. METHOD

3.1. Self-distillation with Task-specific Finetuning

Transformers [17] have recently emerged as an alternative to CNNs, offering superior performance in medical classification tasks [18, 19, 20], with their inherent attention mechanisms providing precise reasoning. However, their limitations are also significant: they require more computational resources and training data, which restricts their applicability in most medical imaging scenarios. We question whether this issue can be mitigated by pretraining the neural network using the visual information contained in unlabeled images.

DINO [8] adopts a similar architecture to most recent SSL-based methods, with the key difference being its use of self-knowledge distillation during training. As shown in Fig 2a, DINO [8] leverages a teacher network g_{θ_t} to guide a student network g_{θ_s} with the same architecture, and θ_t and θ_s are both learnable parameters. During training, the input image \mathbf{x} will be encoded into two sets of \mathbf{K} -dimensional distributions, P_s and P_t . The key difference lies in that the teacher’s input, $\{\mathbf{x}_i^g\}_{i=0}^m$, are more global than the student’s input, $\{\mathbf{x}_j^l\}_{j=0}^n$. In practice, \mathbf{x}^g refers to a larger crop of the original image \mathbf{x} , while \mathbf{x}^l is a smaller, augmented version and we normally set $m > n$. The training objective [8] is to minimize the cross-entropy loss between every P_s and P_t , thereby fostering the correspondence from local-to-global, i.e.,

$$\min_{\theta_s} \sum_{\mathbf{x} \in \{\mathbf{x}_i^g\}} \sum_{\mathbf{x} \in \{\mathbf{x}_j^l\}} H(P_t(\mathbf{x}^g, \tau_t), P_s(\mathbf{x}^l, \tau_s)) \quad (1)$$

where $H(\star)$ is the cross-entropy loss and $P(\star)$ denotes the softmax operation with certain temperature τ which is a non-negative constant. During this process, only the student’s weights g_{θ_s} are updated, while the teacher is updated via exponential moving average (EMA) [21], i.e., $\theta_t \leftarrow \lambda \theta_t + (1 - \lambda) \theta_s$. Notably, [8] shows that **the teacher network produces better features** than the student. Therefore, we will use the teacher for subsequent tasks. It is worth mentioning that the encoded distributions P_s and P_t can be interpreted as the probabilities for the classification over \mathbf{K} predefined classes, whereas our target classes are their subsets. To narrow down from the predefined classes toward LUS scoring, we further perform a fully supervised **task-specific finetuning** on the teacher network using a small set of annotated frames, which

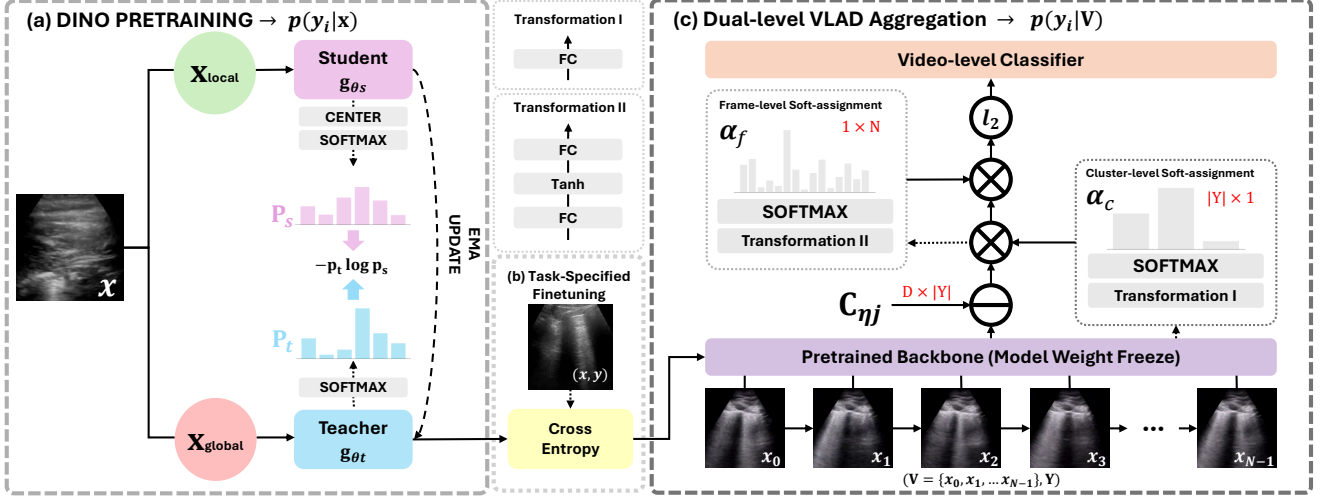


Fig. 2. Overall structure of MeDiVLAD, including (a) DINO-based pretraining on unlabeled frames, (b) optional task-specific finetuning on a small set of labeled frames, and (c) dual-level VLAD aggregation for video-level severity scoring.

we illustrated in Fig. 2b. We denote the finetuned model as $g_{\theta_t}^*$.

3.2. Dual-level VLAD Aggregation

Under our default setting, each ultrasound video contains $N = 15$ frames, where each frame corresponding to an D -dimensional feature vector f , extracted by $g_{\theta_t}^*$. For our proposed dual-level VLDA aggregation (Fig. 2c), we consider the simplest scenario by setting the number of clusters to be equal to the number of labels. Similar to the NetVLAD [11] aggregation, we encode the frame-level ultrasound embedding into a $|Y| \times D$ dimensional feature vector f'_i . This is done by assigning a learned cluster centroid C_{η_j} to every frame embedding and concatenating their residual:

$$f'_i = \left\|_{j=1}^{|Y|} \{ \alpha_c(f_i, j) (f_i - c_j) \} \right\| \quad (2)$$

where $i \in \{1, \dots, N\}$, and $\alpha_c(\star)$ is a learnable cluster-level soft-assignment that assigns frames to clusters based on their proximity. NetVLAD [11] directly measures the sum of f_i across the frame level. However, LUS videos are typically scored based on the highest severity observed in the video. In other words, video-level scoring relies on a single or a few representative frames within the video. To address this, we introduce an additional frame-level soft-assignment denoted as $\alpha_f(f'_i, \tau')$ to perform frame selection. This assignment is implemented through a simple multilayer perceptron (MLP) with tanh activation, where temperature τ' was adopted to control the model's focus on the most informative frame segments. Then, the video-level embedding v is obtained by summing up weighted frame-level features and applying an

intra-normalization σ to suppress bursts [22], i.e.,

$$v = \sigma \left(\sum_i^N \alpha_f(f'_i, \tau') f'_i \right) \quad (3)$$

Finally, a cross-entropy-based video-level classifier is applied to finish the video-level scoring.

4. EXPERIMENTS

Table 1. Experiment Implementation Details

Stage	LR	WD	Epochs	Batch Size	Data
Pretraining	1.25e-4	0.1-0.5	30	64	Unlabeled Frames
Finetuning	5.00e-5	0.001	100	64	Labeled Frames
VideoCls	1.00e-3	0.00001	200	32	Labeled Videos

Given the objective of this work, we did not require a large amount of labeled frame data for training. As such, we performed a 2-fold validation, assigning 302 images from 136 videos to fold 1 and 283 images from 140 videos to fold 2, ensuring that videos from the same source did not appear in different folds. All experiments were conducted on a single Nvidia Quadro RTX 8000 GPU and optimized using the AdamW optimizer, with learning rates decaying according to a cosine schedule. For pretraining, we adopted the ViT-S/8 configuration and data augmentation setup from [8], training the backbone by randomly sampling unlabeled frames from the ultrasound videos. The temperatures τ_t and τ_s were set to 0.5 and 0.1, respectively. Afterward, we finetuned the network on labeled frames in a fully supervised manner. At the video level, we trained the dual-level VLAD aggregation using labeled ultrasound videos. For simplicity, additional training details are summarized in Table 1.

4.1. Image-level Classification

Table 2. Image-level Classification

Methods	Backbone	Pretrain	ROC-AUC	k-NN	Linear
Sup.	ResNet50	IMG	0.793	55.77	63.92
DINO [8]	ViT-S/8	IMG	0.866	57.85	70.57
DINO [8]	ViT-S/8	IMG/LUS	0.878	63.36	75.05
<i>Supervised Finetuning on LUS Image Dataset</i>					
Sup.	ResNet50	IMG	0.863	-	71.94
Scratch	ResNet50	-	0.786	-	64.08
DINO [8]	ViT-S/8	IMG	0.900	-	78.30
DINO [8]	ViT-S/8	IMG/LUS	0.917	-	82.47
Scratch	ViT-S/8	-	0.702	-	58.85

IMG: ImageNet dataset; LUS: Lung-ultrasound dataset

We evaluated MeDiVLAD at the frame level. For this, we trained a ResNet-50 (23.5M) as a classification baseline with a similar number of parameters to the ViT-S (21.7M) we used. The average scoring accuracy (k-NN/linear classifier) and ROC-AUC (one-vs-all) were reported. It should be noted that the k-NN accuracy is only provided for the models that were not fully supervised during training. In the upper half of Table 2, we first examined the impact of self-distillation. Without using LUS data, ResNet-50 pretrained on ImageNet (IMG) showed slightly lower classification accuracy than the other two DINO experiment sets, with the advantage of DINO becoming more pronounced after incorporating unlabeled ultrasound data. As expected, after finetuning the model with labeled frames, both accuracy and ROC-AUC improved, outperforming all other baselines (AUC: 0.917 & Acc: 82.47%). Remarkably, even without supervised finetuning, we achieved an accuracy of 75.05%, surpassing the 71.94% accuracy of the fully supervised ResNet-50. In Fig. 3, we present several attention map visualizations from the finetuned backbone. In (a) and (b), the attention maps accurately highlight both A-lines and B-lines, while in (c), the model identifies all regions of consolidation, offering clear insights into its decision-making process for LUS scoring.

4.2. Video-level Classification

Table 3. Video-level Classification

Methods	Backbone	Pretrain	ROC-AUC	Linear
GlobMAX [4]	ViT-S/8	IMG/LUS*	0.891	75.36
Bi-LSTM [14]	ViT-S/8	IMG/LUS*	0.897	78.59
NetVLAD [11]	ViT-S/8	IMG/LUS*	0.907	77.15
MeDiVLAD	ResNet50	IMG/LUS*	0.866	75.31
MeDiVLAD	ViT-S/8	IMG/LUS	0.888	76.41
MeDiVLAD	ViT-S/8	IMG/LUS*	0.936	82.60

LUS*: Finetuned in a supervised manner with the LUS image dataset.

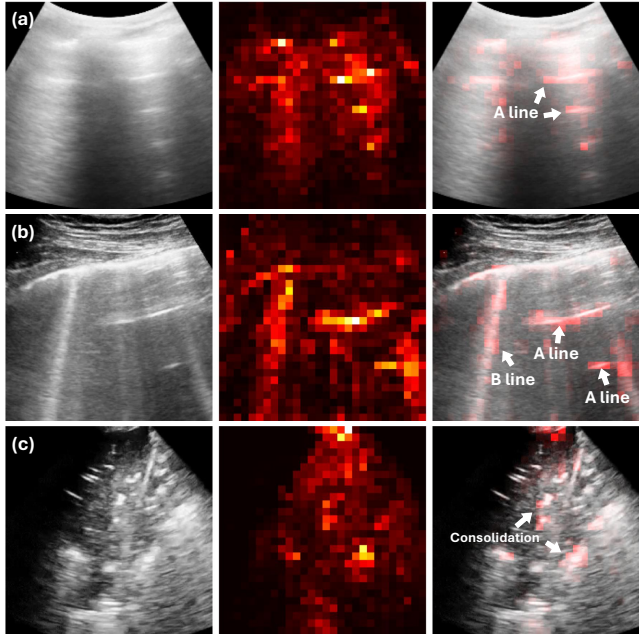


Fig. 3. Typical visualization of attention maps extracted from our pretrained ViT-S/8 (after finetuning).

At the video level, we evaluated our proposed MeDiVLAD aggregation against three typical aggregation methods: Bi-LSTM [14], NetVLAD [11], and directly taking the max severity-category score [4] from the frame predictions. We used the same metrics as in the frame-level experiments for evaluation. For the LSTM, we simply set the hidden size to be the same as the embedding length. Additionally, we performed a grid search to find the best hyperparameters for each model and reported the metrics as the fold average. As shown in Tab. 3, MeDiVLAD significantly outperformed all other methods across all metrics. Similar to the results in the frame-level experiment, using our proposed dual-level VLAD aggregation, we achieved comparable performance to a finetuned ResNet-50, with an AUC of 0.86 versus 0.88 and an accuracy of 75.3% versus 76.4%. These results not only confirm that applying self-knowledge distillation for pretraining a dedicated feature extractor is effective but also demonstrate that using a small amount of annotated data (300 samples) for finetuning can lead to an almost 6% improvement in accuracy.

5. CONCLUSION & DISCUSSION

In this work, we introduced MeDiVLAD, a novel pipeline for LUS scoring at both frame and video levels. By leveraging self-knowledge distillation to pretrain a vision transformer without labels and using dual-level VLAD aggregation, we significantly reduced the reliance on expert annotation. At the frame level, our method achieved 75.05% accuracy without labeled data, which improved to 82.47% with finetuning. At the video level, MeDiVLAD outperformed other aggre-

gation methods, such as Bi-LSTM and NetVLAD. These results highlight the outstanding performance of MeDiVLAD in LUS severity scoring, enabling it to support key applications such as the automatic identification of critical areas in severe lung pathology for further analysis. Furthermore, our pipeline offers a potential solution for broader medical imaging tasks, combining accuracy with interpretability in low-data settings.

6. REFERENCES

- [1] Giovanni Volpicelli, Luna Gargani, Stefano Perlini, et al., “Lung ultrasound for the early diagnosis of covid-19 pneumonia: an international multicenter study,” *Intensive care medicine*, vol. 47, pp. 444–454, 2021.
- [2] Subhankar Roy, Willi Menapace, Sebastiaan Oei, et al., “Deep learning for classification and localization of covid-19 markers in point-of-care lung ultrasound,” *IEEE transactions on medical imaging*, vol. 39, no. 8, pp. 2676–2687, 2020.
- [3] Wufeng Xue, Chunyan Cao, Jie Liu, et al., “Modality alignment contrastive learning for severity assessment of covid-19 from lung ultrasound and clinical information,” *Medical image analysis*, vol. 69, pp. 101975, 2021.
- [4] Gautam Rajendrakumar Gare, Hai V Tran, et al., “Weakly supervised contrastive learning for better severity scoring of lung ultrasound,” *arXiv preprint arXiv:2201.07357*, 2022.
- [5] Mathilde Caron, Ishan Misra, Julien Mairal, et al., “Un-supervised learning of visual features by contrasting cluster assignments,” *Advances in neural information processing systems*, vol. 33, pp. 9912–9924, 2020.
- [6] Ting Chen, Simon Kornblith, Mohammad Norouzi, and Geoffrey Hinton, “A simple framework for contrastive learning of visual representations,” in *International conference on machine learning*. PMLR, 2020, pp. 1597–1607.
- [7] Jean-Bastien Grill, Florian Strub, Florent Altché, et al., “koray kavukcuoglu, remi munos, and michal valko. bootstrap your own latent-a new approach to self-supervised learning,” *Advances in neural information processing systems*, vol. 33, pp. 21271–21284, 2020.
- [8] Mathilde Caron, Hugo Touvron, Ishan Misra, et al., “Emerging properties in self-supervised vision transformers,” in *Proceedings of the IEEE/CVF international conference on computer vision*, 2021, pp. 9650–9660.
- [9] Georgios Petmezas, Vasileios E Papageorgiou, Vasileios Vassilikos, et al., “Recent advancements and applications of deep learning in heart failure: A systematic review,” *Computers in Biology and Medicine*, p. 108557, 2024.
- [10] Hervé Jégou, Matthijs Douze, Cordelia Schmid, et al., “Aggregating local descriptors into a compact image representation,” in *2010 IEEE computer society conference on computer vision and pattern recognition*. IEEE, 2010, pp. 3304–3311.
- [11] Relja Arandjelovic, Petr Gronat, Akihiko Torii, et al., “Netvlad: Cnn architecture for weakly supervised place recognition,” in *Proceedings of the IEEE conference on computer vision and pattern recognition*, 2016, pp. 5297–5307.
- [12] Rongcheng Lin, Jing Xiao, and Jianping Fan, “Nextvlad: An efficient neural network to aggregate frame-level features for large-scale video classification,” in *Proceedings of the European Conference on Computer Vision (ECCV) Workshops*, 2018, pp. 0–0.
- [13] Joao Carreira and Andrew Zisserman, “Quo vadis, action recognition? a new model and the kinetics dataset,” in *proceedings of the IEEE Conference on Computer Vision and Pattern Recognition*, 2017, pp. 6299–6308.
- [14] S Hochreiter, “Long short-term memory,” *Neural Computation MIT-Press*, 1997.
- [15] Ashkan Ebadi, Pengcheng Xi, Alexander MacLean, et al., “Covidx-us - an open-access benchmark dataset of ultrasound imaging data for ai-driven covid-19 analytics,” *arXiv:2103.10003*, 2021.
- [16] Paola Dell’Aquila, Pasquale Raimondo, Vito Racanelli, et al., “Integrated lung ultrasound score for early clinical decision-making in patients with covid-19: results and implications,” *The Ultrasound Journal*, vol. 14, no. 1, pp. 21, 2022.
- [17] A Vaswani, “Attention is all you need,” *Advances in Neural Information Processing Systems*, 2017.
- [18] Yin Dai, Yifan Gao, and Fayu Liu, “Transmed: Transformers advance multi-modal medical image classification,” *Diagnostics*, vol. 11, no. 8, pp. 1384, 2021.
- [19] Xin Wu, Yue Feng, Hong Xu, et al., “Ctranscnn: Combining transformer and cnn in multilabel medical image classification,” *Knowledge-Based Systems*, vol. 281, pp. 111030, 2023.
- [20] Omid Nejati Manzari, Hamid Ahmadabadi, et al., “Medvit: a robust vision transformer for generalized medical image classification,” *Computers in Biology and Medicine*, vol. 157, pp. 106791, 2023.

- [21] Kaiming He, Haoqi Fan, Yuxin Wu, et al., “Momentum contrast for unsupervised visual representation learning,” in *Proceedings of the IEEE/CVF conference on computer vision and pattern recognition*, 2020, pp. 9729–9738.
- [22] Relja Arandjelovic and Andrew Zisserman, “All about vlad,” in *Proceedings of the IEEE conference on Computer Vision and Pattern Recognition*, 2013, pp. 1578–1585.